INTERNATIONAL JOURNAL FOR NUMERICAL METHODS IN FLUIDS
Int. J. Numer. Meth. Fluids **26**: 1023–1038 (1998)

A NUMERICAL INVESTIGATION OF FLOW PAST A BLUFF BODY USING THREE-STATE ANEMOMETRY

M. FUNES-GALLANZI

National Institute of Astrophysics, Optics & Electronics, Puebla, Mexico

SUMMARY

An application of a new flow measurement technique is described which allows for the non-intrusive simultaneous measurement of flow velocity, density, and viscosity. The viscosity information can be used to derive the flow field temperature. The combination of the three measured variables and the perfect-gas law then leads to an estimate of the flow field thermodynamic pressure. Thus, the instantaneous state of a flow field can be completely described. Three-state anemometry (3SA), a derivative of particle image velocimetry (PIV), which uses a combination of three monodisperse sizes of styrene seeding particles is proposed. A marker seeding is chosen to follow the flow as closely as possible, while intermediate and large seeding populations provide two supplementary velocity fields, which are also dependent on fluid density and viscosity. A simplified particle motion equation, aimed at turbomachinery applications, is then solved over the whole field to provide both density and viscosity data. The three velocity fields can be separated in a number of ways. The simplest and that proposed in this paper is to dye the different populations and view the region of interest through interferometric filters. The two critical aspects needed to enable the implementation of such a technique are a suitable selection of the diameters of the particle populations, and the separation of the velocity fields. There has been extensive work on the seeding particle behaviour which allows an estimate of the suitable particle diameters to be made. A technique is described in this paper to allow the separation of particles in a range of micrometer sized velocity fields through fluorescence (separation through intensity also being possible). Some preliminary results by direct numerical simulation (DNS) of a 3SA image are also presented. The particle sizes chosen were 1 μm and 5 μm, tested on the near-wake flow past a cylinder to investigate viscosity only, assuming uniform flow density. The accuracy of the technique, derived from simulations of swirling flows, is estimated as 0.5% RMS for velocity, 2% RMS for the density and viscosity, and 4% RMS for the temperature estimate. © 1998 John Wiley & Sons, Ltd.

KEY WORDS: three-state anemometry; velocity field; particle motion equation

1. INTRODUCTION

As the study of fluid mechanics has evolved, from steady state investigations towards the reality of unsteady phenomena, it has become increasingly clear that instantaneous whole-field non-intrusive flow measurement techniques are required. Particle image velocimetry (PIV) has evolved in recent years to provide such measurements for the velocity field. However, viscosity as well as velocity gradients is required to yield an estimate of the instantaneous rate of loss in turbomachines. The continuing pressure on manufacturers to raise efficiency remains the reason for interest in research into loss generation in turbomachines.

Three-state anemometry (3SA) represents a milestone in terms of the evolution of anemometry techniques [1]. From its origins as a 2D velocity estimation technique, PIV evolved to 3D,

CCC 0271–2091/98/091023–16$17.50

Received April 1996
Revised November 1996

and then to mixtures of seeding being used. For the investigation of two-phase flows, there has been some work done using PIV and two seeding populations [2]. However, in this instance the two populations were 1 μm and 75 μm in diameter, which provided a distinction. Gogineni *et al* [3] also considered using a combination of seeding sizes with their colour PIV system, which employs two lasers, a Nd/Yag and a Nd/Yag pumped dye laser. In this case the two populations were 0.5 μm and 1.0 μm. These two populations were differentiated by the intensity information. A colour film image was obtained and the intensity and colour information was used to eliminate the usual PIV directional ambiguity, and to distinguish between jet and cross-flow information.

Laser induced fluorescence (LIF) has emerged as an attractive technique to measure pressure/temperature. There are different implementations of this technique but the most popular has been that based on an argon-ion laser with iodine as a seed [4]. The argon laser excites iodine molecules that are not in the ground state. Therefore to calculate physical parameters from the measured LIF signal, the optical set-up and laser tuning become rather complicated and difficult to apply for practical flows. Measurements of temperature at a set narrow pressure range have been reported [5]. Pressure and velocity measurements, based on the Doppler shift of the fluorescence spectral lines, at a set narrow range of temperatures [6] have also been reported. The main problem with this technique is the cross dependence of the fluorescence on pressure and temperature.

For turbomachinery applications, pressure and temperature vary simultaneously over wide ranges, in an enclosed surrounding, and using a gas with a high expansion rate. Although there has been some variants which show good promise, the technique of LIF remains problematic and untried in turbomachinery. However, the basic idea of seeding a flow with fluorescent seeding to obtain more than just velocity estimates is attractive. Furthermore, one of the most difficult experimental problems with PIV is that of glare from near surfaces. Through the use of fluorescent particles and interferometric filters, this effect can be minimised. In fact, fluorescent seeding has been shown to work in conjunction with PIV [7,8].

The tracking capability of scattering particles is essential for reliable velocity measurements with laser anemometry. The study of the sizing criteria for laser anemometry particles is now highly refined and has been the subject of several articles [9–11]. Therefore the correct particle size for a faithful flow-following can be reliably ascertained.

There are many aspects of loss generation in turbomachinery which need further extensive research. Given that efficiency for turbines is already in the region of 90%, the areas where losses are generated and the magnitude of these effects is small and difficult to investigate. The efficiency achieved to date is primarily due to the fact that turbine flow is dominated by the laws of conservation of mass, energy and momentum. Thus, the remaining sources of loss are mainly related to viscous effects and secondary flow. Denton [12] has recently suggested that understanding would be improved by looking at loss in terms of entropy generation. Studies of the relationship between viscous forces and entropy creation show that the entropy creation rate is likely to be high in regions where high velocities coincide with high viscous forces. These two factors are likely to result in rotation, dilation and shear strain. The rate of shear can be measured directly on full-size turbine vanes, economically and non-intrusively.

PIV results of a turbine wake and related vortex structure in a hostile industrial environment have been reported in the literature [13]. High speed 3D PIV measurements [14] using the seeding optical characteristics to provide an accurate 3D data field have also been achieved. This approach provides more accurate 3D PIV information and, more importantly, enables the classification of particle data according to particle size. Furthermore, while homologous relationships allow the investigation of turbomachines through models, they do not permit

viscous forces to be scaled properly; hence there is a slight difference in the efficiency of various sizes. The larger the machine, the more efficient it is, but the difference is normally not more than 2–3%. Therefore, in order to obtain the most reliable results, experiments have to be performed on full-size vanes at operating conditions.

The combination and refinement of anemometry techniques implied in 3SA which for the first time may provide instantaneous velocity, density and temperature whole-field estimates, opens the way for a detailed investigation of mixing processes and unsteady effects. Some initial results obtained from computer simulations are described in this paper, together with some limitations of the technique and the current areas of development and testing.

2. PARTICLE MOTION EQUATION

All analyses of particle motion using PIV assume spherical particles. This is a valid assumption, as the particles used for transonic flow research are often sub-μm styrene. Polystyrene latex spheres are a popular seeding material with a specific gravity of 1.05. They are relatively easy to manufacture in large quantities to any size in the range 0.3–10 μm [15]. Styrene, in particular, has a very high scattering cross-section which allows the imaging of particles down to 0.2 μm. These are the main factors as far as the light scattering characteristics are concerned. The aerodynamic behaviour depends on its inertia and the drag force. A common parameter for aerodynamic and scattering characteristics is the particle diameter. Interference between particles is neglected because the highest concentrations employed are too low for such effects. For flow-following capability, subject to a prescribed tolerance, the diameter can be specified.

Together with the fluid velocity gradients, the most important influences on particle motion are the particle diameter d_p, the particle and fluid densities ρ_p and ρ_f, and the viscosity μ. An analysis of the relative motion of particle and fluid yields the following dimensionless equation as an approximation [16]:

$$\frac{\mathrm{d}v_i}{\mathrm{d}t}+\frac{1}{2}\beta\frac{\mathrm{d}}{\mathrm{d}t}\left(v_i-u_i-\frac{1}{10}\delta^2u_{i,jj}\right)+\left(v_i-u_i-\frac{1}{6}\delta^2u_{i,jj}\right)$$
$$+\sqrt{\frac{9\beta}{2\pi}}\int_0^t\frac{\mathrm{d}/\mathrm{d}t\ (v_i-u_i-1/6\ \delta^2u_{i,jj})}{\sqrt{t-\sigma}}\,\mathrm{d}\sigma=(1-\beta)\frac{2\rho_p\alpha^2}{9U_0\mu}g_i+\beta\frac{\mathrm{D}u_i}{\mathrm{D}t} \tag{1}$$

The operator $\mathrm{d}/\mathrm{d}t$ denotes a derivative following the particle and $\mathrm{D}/\mathrm{D}t$ a derivative following the fluid. In creeping flow these two derivatives are approximately the same. The characteristic time and fluid velocity have been used to make the fore-going equation dimensionless. The Laplacian operator is made dimensionless by the characteristic distance L of the flow. α is the particle radius, β is the dimensionless density and δ is the ratio of the dimensions α/L. The subscripts f and p refer to the fluid and particles respectively. Moreover, slip on the sphere diminishes the effect of the history term in the determination of the instantaneous velocity of the sphere [17].

For turbomachinery flows, the characteristic distance of the flow might be based on chord length, and Reynolds number calculated on the basis of the characteristic fluid velocity; and are generally in the 1.2e + 06 range, e.g. stator vanes. For seeding particles, the effective Reynolds number is calculated based on the particle diameter and slip velocity. Therefore, μm-sized particles can be considered to exhibit creeping flow behaviour in turbomachines. This leads to a considerable simplification of the above equation which makes it possible to carry

out 3SA measurements and numerical simulations. The simplified equation of motion can then be expressed in terms of viscosity and fluid density which are the required unknowns. Thus, if a combination of particle sizes is used to seed the flow, both the instantaneous fluid velocity field and each particle sub-group velocity field can be ascertained. By using a marker particle size designed to follow the flow accurately, together with two other sub-group sizes, it is possible to solve a system of simultaneous equations of particle motion to yield density and viscosity.

The viscosity data field can be transformed to yield a whole-field temperature estimate. This temperature estimate can then be combined with the density estimate to yield, through the use of the perfect-gas law, a whole-field thermodynamic pressure estimate. The seeding size distribution can be controlled to ensure a monodisperse population. For instance, at 1 μm a typical seeding batch, produced at the Department of Chemistry of the University of Warwick, has 95% of the particles between 0.9 and 1.1 μm. Accuracy bounds are valid for the data range applicable for turbomachinery applications and assuming air is the fluid being investigated. These are arrived at from an error analysis of the simultaneous equations and allowing a further error arising out of the spatial interpolation. A detailed analysis of the expected accuracies cannot be obtained analytically, owing to the large number of factors involved (seeding distribution, velocity gradients, measurable velocity dynamic range, pulse separation, heat transfer conditions, seeding size distribution, etc.) and because accuracy estimates are dependent on the flow characteristics. The estimates mentioned in this paper were derived from simplified simulations of swirling flows.

3. SEEDING MIXTURE

The compromise concerning the size of the intermediate and large particle sub-groups requires extensive research to determine the optimum sizes and proportions in the seeding mixture. The larger particles would provide more sensitivity to viscosity and ease the particle population discrimination requirement to be able to separate the three velocity fields. On the other hand, the smaller the particles will follow the flow more closely and provide a more detailed coverage of the field for all three-state variables.

Dring and Suo [10] showed that the nature of a particle trajectory in a free-vortex swirling flow is, to a large degree, governed by the Stokes number (St). When $St < 0.1$, the particle will closely follow the circular fluid streamlines. When $St > 1.0$ the particle will be ultimately centrifuged out across the fluid streamlines in swirling flows. For particle Stokes values higher than 0.1 in high Reynolds number flows, two extra parameters are required to describe the nature of the particle trajectory; one essentially dependent on viscosity and the other on density. For example, by raising the diameter of seeding from 0.4 μm to 4.0 μm, the Stokes number is increased 100-fold, making the larger populations dependent on fluid density and viscosity. The Stokes number consideration determines the upper particle size limit, while discrimination between particle velocity fields determines the lower bounds.

Research now centres on the optimum composition for turbomachinery research. Seeding distribution across the flow field will be more uniform for the marker population than for the others. Therefore, the seeding mixture has to take this into consideration and increase the marker seeding proportion.

The reflectivity of the seeding particles is, however, a major aspect of the seeding mixture requirements. The imaging is performed with the use of digital CCD technology. Although CCD is more sensitive than film, its dynamic range is two orders of magnitude smaller.

Therefore, the reflectivity of the larger particles must be adjusted to bring the intermediate and large particle sub-groups back into a range that the CCD can image without saturating, and to ensure separability of the convolved velocity fields. Four processes are possible on the polystyrene resins currently being investigated, namely dyeing, fluorescence, phosphorescence and grey level information.

The marker polystyrene is more difficult to inject with additives but particles above 1.0 μm can easily have additives. Therefore, the easiest way to discriminate between the populations is to make the larger seeding populations fluoresce at different frequencies in order to distinguish between the three velocity fields. This is the approach being pursued with a set-up as shown in Figure 1. In this arrangement two simultaneously triggered CCD cameras are employed, looking at the region of interest through a beam-splitter arrangement. In the general case, one of the three populations appears in both views together with one of the other two in each of the two images. Narrow-band filters must be used to reject the uniform background fluorescence likely to appear on the blade surfaces, walls, etc. Previous experience with 10-nm bandpass filters has shown that image contrast can be reduced because of the collection of more background fluorescence. Dyeing is required to bring the dynamic range of the three populations within that of the CCD cameras for the case of characterisation by grey levels.

The system shown will be tested with styrene doped with Fluorescein dye (514.5 nm) and Rhodamin-B (575 nm) and viewed through two interferometric filters after separation by the beam-splitter. Since the spectra of the dyes overlap, there is a calibration step involved to separate the two populations. The light sheet is created with an Argon ion laser ($\lambda = 488$ nm). This arrangement has been described previously in the literature [18] in an application involving simultaneous measurements of two species concentrations in turbulent flow by planar LIF.

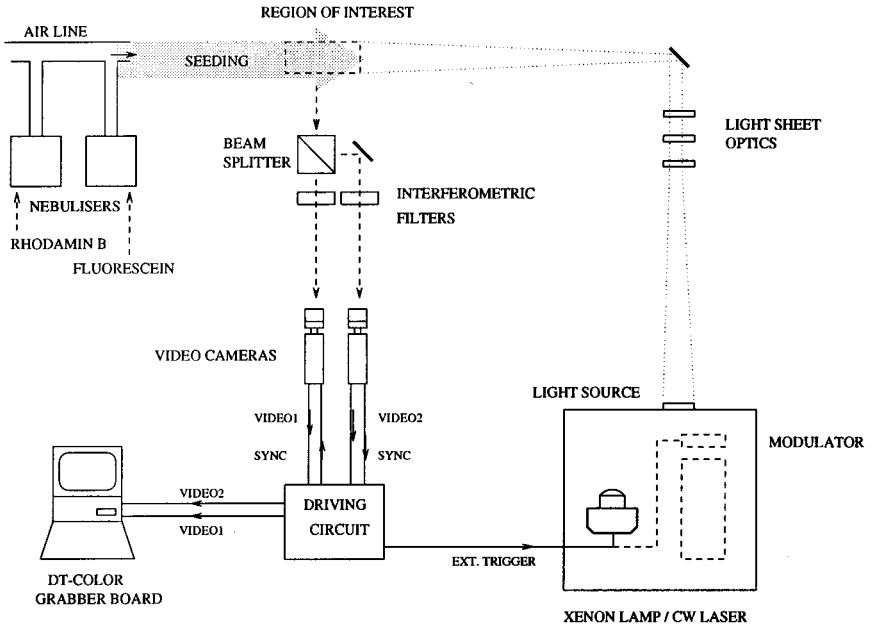

Figure 1. Schematic diagram of CCD-based 3S system.

The melting temperature of styrene is 250°C, and its glass transition temperature is 90°C, so it is currently applicable to turbomachinery running at up to 90°C. However, a facility such as the DRA Pyestock ILPC, which is capable of running at full engine representative conditions—matching both heat transfer and aerodynamic information—requires a temperature of 190°C. Therefore, a new high temperature version of the resin has been made which is highly cross-linked and can stand up to a temperature of ≈ 200°C. Further study is being made of alternative and complementary materials.

4. STOKES NUMBER

Previous calculations of flow-following capabilities of seeding particles have in general assumed potential flow and a constant value for the viscosity coefficient. However for turbomachinery applications, if viscosity changes, geometric considerations and flow characteristics are considered, it is clear that there is not a single but a set of flow conditions which must be considered when e.g. investigating flow through a turbine stage. The Stokes number can be defined as:

$$St = \frac{\rho v_c d_p^2}{18 \mu L_c} \tag{2}$$

Thus, regions of high viscosity aid seeding flow-following by locally reducing St. For example, at the edge of separated regions, the effective viscosity may be 100 times the laminar viscosity found mid-passage. Therefore, the seeding would behave as if it was 1/10th of the diameter. More specifically, the turning angle encountered by the seeding on the pressure side of a stator vane for instance, is made easier to follow by the increased viscosity at the leading edge of the blade. On the suction, however, the turning angle required is higher and the viscosity lower. The Stokes number for a stator vane can be defined as:

$$St = \frac{\rho_p v_u d_p^2}{18 \mu C} \tag{3}$$

So, typically for a stator vane, at 300 m s^{-1} with a 1% error on the pressure side, a particle diameter of 0.7 μs is required. On the suction side however, a diameter of 0.4 μs is necessary owing to viscosity and turning angles considerations.

From a Eulerian frame of reference, the wake represents an oscillation at a frequency given by the vortex shedding frequency. The Stokes number in this case can be defined as:

$$St = \frac{\rho_p \omega d_p^2}{18 \mu} \tag{4}$$

Assuming a vortex shedding frequency of 36 kHz based on blade thickness at the trailing edge plus the boundary layer momentum thickness, and a mean velocity of 300 m s^{-1}, results in a seeding diameter requirement of 0.2 μs.

Owing to the fact that further downstream in the rotor section, both the previously mentioned considerations regarding pressure/suction surfaces apply, and because of the rotor movement and geometry, it is easier to treat this part of the flow as if it consisted of swirling flow. In this case, the entry angle, exit angle, relative velocities, and rotor curvature are needed. The Stokes number can then be defined as:

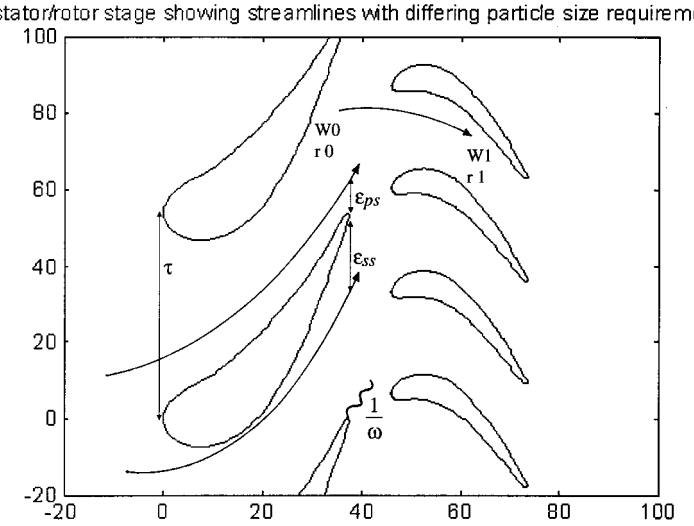

Figure 2. Particle size requirements for a turbine stage.

$$St = \frac{\rho_p W_0 d_p^2}{18 \mu r_o} \tag{5}$$

So there are at least four clearly defined regions of flow where the correct size of seeding has to be assessed differently (see Figure 2). Thus, the composition of the seeding mixture has to be specified, bearing in mind the region of interest. The most difficult is the wake region downstream of the stator, while the least difficult is the region applicable to flow around the rotor section.

5. VELOCITY ESTIMATES

At high speeds, due to the low seeding density and small scale information contained in regions of interest, e.g. wakes or boundary layers, the spatial approach to PIV is preferred. Due to the large data compression, this allows an intensive amount of processing to be performed on any identified particles. Due to the well-known geometric difficulties with 3D data, an approach which makes use of the particle grey level information to obtain an accurate estimate for the out-of-plane velocity component; as well as sub-pixel accuracy in the light-sheet plane has been developed. This enables the use of small angles between the viewing cameras.

A diffraction-limited optical component is used to provide aberration-free particle images. The sensitivity of the CCD cameras and hardware is altered with the use of bespoke tuning for laser operation. It is possible to record doublets with a lower displacement than in the past, leading to an increase in dynamic range. The particle data can be automatically analyzed in software. Using CCD technology at only 768×576 pixel resolution, PIV data of the order of 700 points has recently been obtained. It is estimated that in order to separate three velocity fields with velocity accuracy of the order of 0.5%, at least 1000 measurement points should be obtained for each field, and possibly more if high velocity gradients are to be investigated. This is a starting assumption and a demanding accuracy which would require the use of high precision position estimation techniques, such as those due to Havelock [19] and recently applied to PIV data [20]. Clearly, if this assumption cannot be met, all the accuracy estimates

must be scaled accordingly. Therefore, combined with high accuracy techniques, a 12-bit 2048×2048 digital camera will also be required to make accurate measurements for industrial applications if grey level information is required, and 8-bit would be sufficient for velocity fields separated by fluorescence.

3SA arrives at a velocity measurement by dividing the displacement, which has a given absolute error, by the pulse separation. Therefore, areas of low relative speed tend to have estimates of velocity with correspondingly large errors, but these are few in number because seeding density can be considered to depend linearly with speed as a first approximation. On the other hand, areas of high velocity yield a large number of high-accuracy velocity estimates leading to redundancy and thus inconsistency in the quality of the data across the image. By exploiting the spatial coherence of the data, an interpolation method can be derived which is more accurate than individual data points and homogeneous in terms of its error profile. This is achieved by considering the conditioning of the approximating matrix in relation to the seeding density and characteristics of the measurement system employed. The large number of velocity samples mentioned are required to provide well-conditioned velocity field matrices.

A limitation of the 3SA technique is that the larger particle sub-groups do not follow the flow as closely as the flow marker particles by definition, and therefore some regions of the flow would not be suitably covered by all three seeding populations. In regions of high turning or back flow, it is very difficult to inject seeding at all, and if the velocity is very low, the dynamic range constraints would have to be altered together with the seeding rate. Therefore, regions of high velocity gradients remain a challenging area of research. This limitation might be overcome by complementing 3S data with CFD calculations to help fill in the detail. Figure 3 illustrates the problem for the case of a swirling flow. For the case of a particle with $St < 0.1$, the normalized position after a 90° turn would be a little over 1.1, whereas for a particle with $St = 10$ the equivalent position would be 2.2. Therefore, this dead-zone region would not be covered by the larger population.

6. DENSITY, VISCOSITY AND PRESSURE ESTIMATES

Aerodynamically the pressure dependence of air viscosity can be ignored and considered to depend only on temperature variations. The expected accuracy for the viscosity and density estimates is of the order of 2%. For routine calculations in air an approximation by Sutherland can be used [21]. The error of the temperature estimate is the same as that for density, plus that involved in using an approximation to provide the temperature data from viscosity information. Thus, for the current set-up, the accuracy of the temperature estimate is 4%. Density measurement has not yet been attempted or even simulated, and so remains an area to be further investigated. However, the main variables of interest are the velocity field and the viscosity, from which the instantaneous rate of entropy generation can be derived. Therefore, this is not expected to delay development of the technique.

Over the range of values applicable to turbomachinery flow, the perfect-gas law is accurate to $< 1\%$ error. Therefore, the temperature and density fields can be combined to derive a thermodynamic pressure field. Thus, the flow under study can potentially be described completely.

Due to the combination of factors involved in making the pressure field estimate, an accuracy in the range of 5–10% is expected. However, such an estimate would be almost instantaneous. Typically, the pulse separation for turbomachinery research is of the order of 0.5 μs. This method of arriving at an estimate of pressure yields the thermodynamic pressure.

7. DISCUSSION

Both the frequency and spatial techniques for PIV can be employed to obtain density and viscosity estimates. On the other hand, the nature of the frequency technique negates any possibility of investigating the smaller scale structures in the flow. The spatial technique can resolve fine small scale detail even in low seeding regions, but it requires the use of sophisticated algorithms due to the irregularly spaced velocity data field. Moreover, the spatial approach cannot deal on its own with high seeding densities and/or high-turning flows. However, using an integrated approach of splitting the image into tiles and using the result of the frequency analysis as the initial condition for an iterative spatial processing of individual pairs, any type of data field can be analyzed down to small scales with high accuracies.

Despite its current limitations, the technique provides for the first time a viable whole-field instantaneous means of obtaining all three-state variables from a single measurement. In mixing studies for instance, both velocity and a scalar property, e.g. temperature or species concentration, are to be determined. A technique such as 3SA will enable CFD code for mixing to be validated.

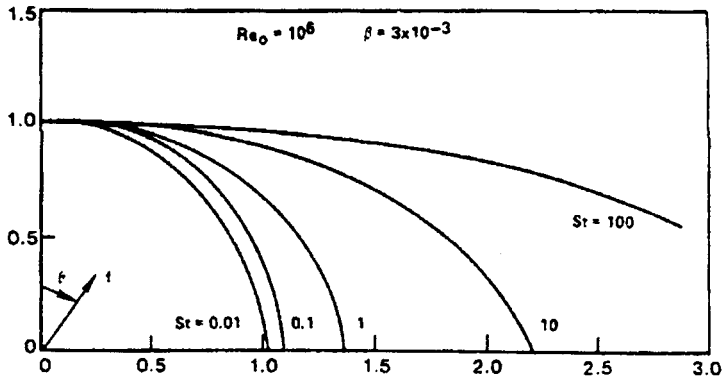

Particle trajectories for $Re_0 = 10^6$.

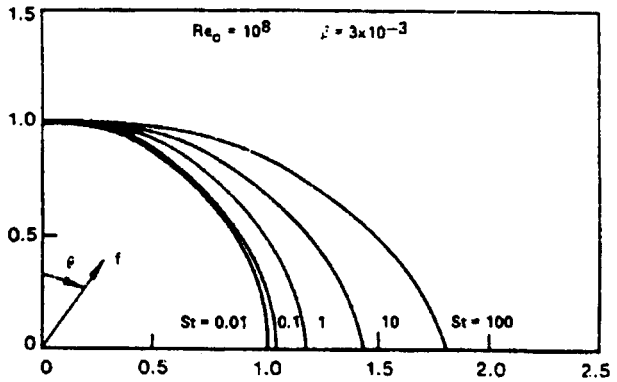

Particle trajectories for $Re_0 = 10^8$.

Figure 3. Swirling flow (taken from Dring [11]).

Like PIV, 3SA can only measure a limited range of velocities. Currently, using the spatial approach, it is possible to achieve a ratio of the largest to smallest velocity of the order of seven. Thus, if the middle velocity for which the optimum pulse separation was chosen was 200 m s^{-1}, a measurement range of 50–350 m s^{-1} would be possible. Therefore, this measurement range would be adequate for the likely velocity gradients present in transonic flows. Regions of high entropy generation would also be difficult for the larger seeding populations to enter however, therefore it may not be possible to make 3SA measurements e.g. inside the near-wake region behind trailing edges. These regions also tend to be areas of high viscosity, in some instances up to 100-fold higher, which would help to keep the larger particles in, but a comprehensive investigation of this issue has not yet been completed.

A technique providing an instantaneous snapshot of all three-state equations could lead to a complete measurement flow model and the subsequent increases in efficiency. In order to estimate the instantaneous rate of entropy generation, as described earlier, only the rate of shear and the viscosity are required. Therefore, it could be estimated with an accuracy of the order of 5% (or an order of magnitude almost more accurate than the best current CFD estimates for an attached boundary layer).

8. PRELIMINARY RESULTS

The validation procedure for this technique can be separated into four steps. The first consists of developing a method to deconvolve the three sub-group velocity fields. The second involves the use of computer simulations on a modelled flow to investigate the correct proportions, size and characteristics of the seeding required for turbomachinery applications. The third stage will consist of making experimental measurements of the well-known flow in the near-wake of a cylinder or wedge, and comparing them with the simulated data. Finally, the development will involve the testing of the technique on a practical industrial flow.

The first stage of the validation process has been completed. Monodisperse fluorescent styrene particles have been produced. Interferometric filters can discriminate between the seeding dyed with Fluorecein and that dyed by Rhodamin-B; though other dyes are also being investigated. Further work is currently under way to try to discriminate using the grey level information. In this way, the two-camera arrangement will be used to provide 3D information, rather than a beam-splitter arrangement which only yields 2D information.

As part of the research program on 3D PIV, the author has produced an integrated software package to validate and simulate PIV data [1]. This consists of three parts: the first is a CFD code based on the NSC2KE code by INRIA [22] together with an unstructured grids mesher, the second is a particle-imaging code, and lastly a particle velocity field estimation code which is still under active development [28].

8.1. Modelled flow

The second stage, involving the simulation of a flow past the near-wake of a cylinder, has also been completed and is described in this paper. For this case, the density is assumed to remain constant and therefore only two seeding populations are needed. A first order approximation [23] to the particle motion equation reduces Equation (1) to:

$$\frac{\mathrm{d}v_\mathrm{p}}{\mathrm{d}t} + av_\mathrm{p} = av_\mathrm{f} + b\frac{\mathrm{d}v_\mathrm{f}}{\mathrm{d}t} \tag{6}$$

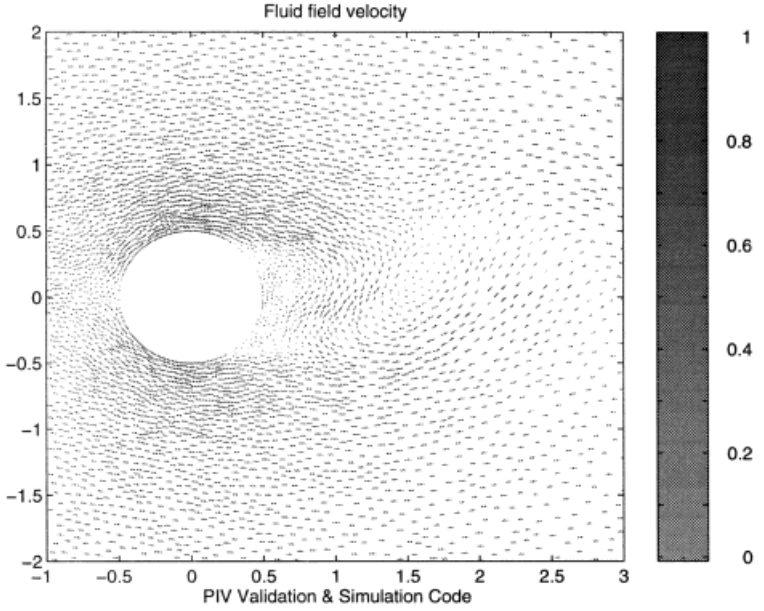

Figure 4. Predicted cylinder flow velocity field.

where $a = 36\mu_{ij}/(2\rho_p + \rho_f)d^2$ and $b = 3\rho_f/2\rho_p + \rho_f$.

As previously mentioned, if creeping flow is assumed (technically $Re < 1.0$ but is still broadly similar for $Re < 5.0$ [24], then D/Dt and d/dt are approximately equal. This can be combined with the inclusion of small diffusion terms to yield:

$$\frac{\partial v_p}{\partial t} + u\frac{\partial v_p}{\partial x} + v\frac{\partial v_p}{\partial y} + av_p - k1\frac{\partial^2 v_p}{\partial y^2} - k2\frac{\partial^2 v_p}{\partial x^2} = av_f + b\frac{dv_f}{dt}. \tag{7}$$

The diffusion terms can be justified on physical grounds relating to the pressure drop in the surrounding fluid, but their real purpose is to damp down any artificial diffusivity resulting from the numerical simulation. Equation (7) then becomes an almost straightforward transport equation. It was solved by a split formulation and the application of the Galerkin finite element method with bilinear rectangular elements, to solve the unsteady particle velocity problem [25]. The program was used to solve for different particle diameters and provide a particle velocity field. By including the viscosity tensor in the particle velocity field calculation, the heat transfer and aerodynamic characteristics of the flow are coupled.

Flow past the near-wake of a cylinder at a Reynolds number of 140 000 is being used as test flow because experimental aerodynamic data is available for validation purposes. Direct numerical simulation data was used to produce a simulated 3SA image, with particle imaging partly based on the description by Adrian [26], and was then deconvolved and analyzed. The CFD calculation used a Navier–Stokes second order scheme, Roe solver and the isothermal wall model. The turbulence model used was a k–ε model and wall laws. The experimental parameters considered were a cylinder 10 mm in diameter with a mean flow velocity of ≈ 100 m s^{-1}.

For the flow under consideration, only the viscosity is a variable in the derivation of the particle velocity fields. Therefore, only two sizes of particle are required to fully describe the flow under consideration. Figure 4 shows a plot of the flow being investigated. Figure 5 shows

the particle velocity field for a 5 μm particle and a close-up CFD view of the near-wake region. The particle velocity field for a 1 μm particle, where $St = 0.1$, varied by 1% RMS from the computed velocity field in the u-direction, as expected from experimental data. The 5 μm particle velocity fields differed by 6.7% in the u-direction and 13.4% in the v-direction. Its Stokes number is 2.5 and as can be seen from Figure 3, ultimately it would be centrifuged out in a swirling flow.

8.2. Simulated three-state anemometry image

The CCD imaging modelled was that of a 2048×2048 8-bit system. The simulated 3SA image contained ≈ 1000 samples per seeding population. This is the result of a seeding rate of 1 particle mm^{-3} upstream. The seeding density was set proportionally to flow velocity, as a first order approximation. The combined particle images of the two fields than had CCD noise added. The CCD noise came from a real shot at the previously mentioned conditions in a Ludwieg tube. The particle imaging assumed a light-sheet thickness of 1 mm.

The region of interest, at a magnification of one, was set to 25×25 mm, at a distance of 600 mm; 1 mm behind the cylinder to provide a clearance to ensure there would be no glare from the laser light hitting the cylinder surface when the experiment is performed. A close-up region of the combined 3SA image is shown in Figure 6. Note the differing size and intensity of the two populations, which is due to the difference in relative sensitivity of the CCD camera and the diffraction-limited spot size for the two populations at 488 nm and 575 nm.

8.3. Image analysis

The two deconvolved particle fields were analyzed using the Analysis by Integrated Processing (AIP) package. AIP is a computer program which is the result of a long period of research directed towards the automatic extraction of particle image data from stored digital images. An integrated processing method was adopted. It is currently in use by the author in applications involving low- and high-speed flows, as well as secondary flow research in a

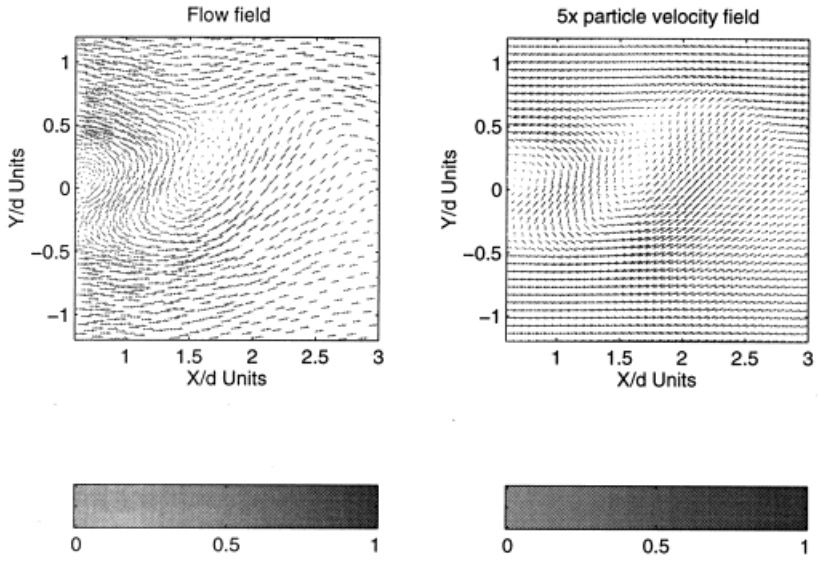

Figure 5. CFD velocity field/5 μ particle field.

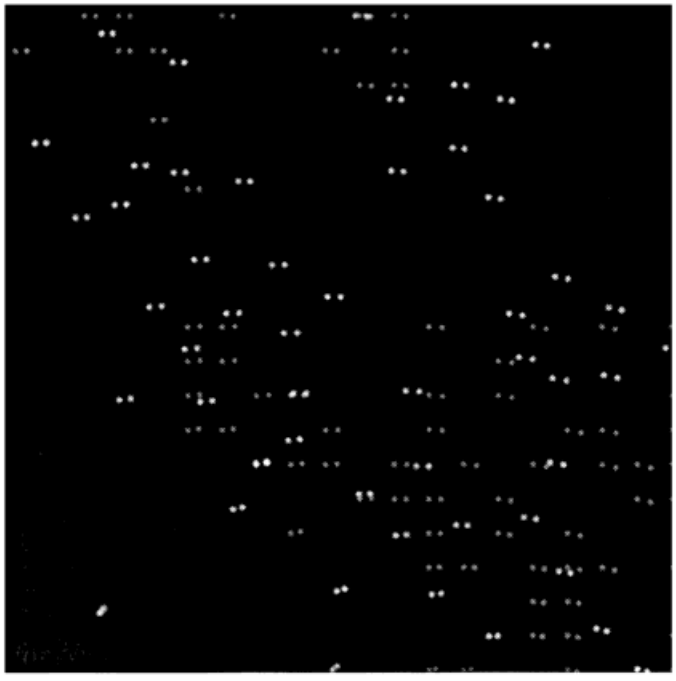

Figure 6. Simulated combined 3SA image with added

two-stage turbine facility. This code differs from that reported previously in the literature due to following changes:

- The method now uses an integrated approach, the frequency technique is used in a first sweep to yield rough estimates and then the spatial approach is applied iteratively to small regions of the flow, called tiles.
- The second change is that the 'locales approach' is used for particle position estimation [20]. This approach involves sub-pixel position estimation, considering not only the spatial discretization information, but also intensity discretization, rather than the Gaussian fit previously reported.
- A detailed method of dealing with sources of error and their minimization by calibration has now been implemented in the software.
- Data display and measured data rate parameters are related to the Kolmogorov scales and matrix conditioning. In this way comparable plots can be made with data obtained from experiments with different data rates and at different scales.

The quoted RMS error values are not indicative of the likely accuracy of the viscosity estimate because the error value is global whereas the changes due to the viscosity occur only in a sub-region. In large parts of the area, the errors remain low irrespective of the particle size. Furthermore, the accuracy of the measurement is sensitive to the flow velocity gradients and geometry. The error of the inferred to the computed viscosity was 6% RMS for the cylinder flow under the aforementioned conditions. A wake flow such as the one described is more challenging than a swirling flow, and since the model included the varying seeding concentrations through the field, together with all the other modelled factors, all these effects contributed to the higher than expected error. A value for the viscosity was obtained in the u- and

v-direction and averaged to arrive at the final estimate. The actual experimental results can be expected to be very close to those of the simulation, since all important factors were taken into consideration. Many aspects of the technique, however, can be expected to be improved and so the theoretical accuracies for swirling flows are the long-term goal. The viscosity could be combined to the flow rate of shear to yield an instantaneous estimate of the rate of entropy generation.

A further study will commence shortly, concerning computed flow around a wedge profile in the transonic region, where both temperature and density changes occur. This work has been previously investigated by comparisons with interferometric measurements [27] and therefore can be used as a benchmark. Thus, from the computed flow, a simulated image will be generated by inserting into the computed flow three different particle sizes. This 3SA image will then be subjected to the process of velocity fields deconvolution and the resulting temperature and pressure estimates will be compared with the calculated and experimental data. The fourth stage is expected to be achieved over the next three years.

9. CONCLUSIONS

PIV has been previously successfully tested for high-speed unsteady non-intrusive measurements in turbomachinery. 3SA is a development of, and experimentally very similar to, PIV and so would be applicable to either compressor or turbines. It provides, for the first time, a means of instantaneously estimating all three-state variables, enabling a full description of the flow. It is therefore directly applicable to mixing and trailing edge loss, investigation of leading edge shocks in gas turbine compressors, stator/rotor interactions, and the validation of CFD codes; assuming enough seeding is able to enter the region of interest.

The theory of the technique is fully described. Much work remains to be done to make this a practical method but the potential rewards make it worthwhile. The results shown in this paper prove the theoretical feasibility of the technique.

Progress towards a 3D measurement of velocity, density and temperature for a steady flow is feasible in the foreseeable future. The expected experimental accuracies for benchmark swirling flows are 0.5% for the velocity field, 2% for the density and viscosity fields, and 4% for the temperature estimates. Therefore, 3SA (if experimentally validated for the likely velocity gradients in regions of high loss) would be able to derive an estimate of the whole-field instantaneous rate of entropy generation, a measurement which cannot currently be done by any means.

APPENDIX A. NOMENCLATURE

C chord
d blade thickness at the trailing edge
L characteristic distance of the flow
M molecular weight
Re Reynolds number
S_a entropy creation rate/unit surface area
St Stokes number
T static temperature
p thermodynamic pressure
v velocity

Greek symbols

α particle radius
β dimensionless density
δ ratio of the dimensions α/L
ε defined in Figure 2
λ Lamé constant
μ viscosity
θ boundary layer momentum thickness
ρ fluid density
σ collision diameter
τ blade pitch
Ω collision integral
ω vortex shedding frequency

Subscripts

c characteristic
f fluid
p particle
ps pressure side
ss suction side
u upstream

REFERENCES

1. M. Funes-Gallanzi, 'A novel fluids research technique: three-state anemometry', *ASME*, June 10–13, 1996, 96-GT-305, Birmingham NEC, UK.
2. D. McCluskey, A.K. Hind, S. Rix and C.A. Greated, 'Development and Application of a Simultaneous Two Phase PIV System for the Analysis of Air-Particle Flow Fields', C485/048, *Proc. Optical Methods and Data Processing in Heat and Fluid Flow*, IMechE, London, UK, 1994.
3. S.P. Gogineni, D.D. Trump and L.P. Goss, 'PIV measurements of a jet in a cross flow', *ASME FED*, **218**, 71–80 (1995).
4. J.C. McDaniel, 'Investigation of laser-induced iodine fluorescence for the measurement of density in compressible flows', Stanford University, SUDAAR No. 532, 1982.
5. M. Inoue, M. Masuda, M. Furukawa and T. Muraishi, 'Diagnosis of three-dimensional transonic flow fields with laser-induced iodine fluorescence', *ASME FED*, **218**, 163–170 (1995).
6. F. Lemoine, X. Lefevre and B. Leporq, 'Pressure and velocity measurements in compressible flows using iodine fluorescence induced by a single-mode laser', *ASME FED*, **218**, 81–87 (1995).
7. M.A. Northrup, T.J. Kulp and S. Michael Angel, 'Fluorescent particle image velocimetry: application to flow measurement in refractive index-matched porous media', *Appl. Opt*., **30**, (1991).
8. O.G. Philip, W.D. Schmidl Y.A. Hassan, 'Development of a high-speed particle image velocimetry technique using fluorescent tracers to study bubble collapse', *Nucl. Eng. Des*., **149**, 375–385 (1994).
9. A. Melling, 'Seeding gas flows for laser anemometry', AGARD, Conference Proceedings 395, 1986.
10. R.P. Dring and M. Suo, 'Particle trajectories in swirling flows', *AIAA J. Energy*, **2**, 232–237 (1978).
11. R.P. Dring, 'Sizing criteria for laser anemometry particles', *J. Fluids Eng*., **104**, 15–17 (1982).
12. J.D. Denton, 'Loss mechanisms in turbomachines', *ASME*, 1993, 93-GT-435.
13. M. Funes-Gallanzi, P.J. Bryanston-Cross and K.S. Chana, 'Wake region measurement of a highly three-dimensional nozzle guide vane tested at DRA Pyestock using particle image velocimetry', *ASME*, 1994, 94-GT-349.
14. M. Funes-Gallanzi, D.D. Udrea and P.J. Bryanston-Cross, 'Advances of the warwick real-time digital 3DPIV system for turbomachinery research', *ASME FED*, **218**, 1995.
15. C.E. Nichols, Jr., 'Preparation of polystyrene microspheres for laser velocimetry in wind tunnels', NASA TM-89163.
16. M.R. Maxey and J.J. Riley, 'Equation of motion for a small rigid sphere in a non-uniform flow', *Phys. Fluids*, **26**, 883–889 (1983).

17. E.E. Michelides and Z.G. Feng, *Int. J. Multiphase Flow*, **21**, 315–321 (1995).
18. L. Brocquet and S. Simoens, 'Simultaneous measurements of two species concentrations in turbulent flow by planar laser induced fluorescence', *EUROMECH Colloquium 335-Image Techniques and Analysis in Fluid Dynamics*, Rome, 5–7 June, 1995.
19. D.I. Havelock, 'High precision position estimation in digital image metrology', *Ph.D. Thesis*, Carleton University, Dept. Syst. Eng. Comput. Sci., Ottawa, Canada, July 1989.
20. M. Funes-Gallanzi and F. Mendoza Santoyo, 'Analysis by integrated processing of unsteady flow PIV data', 1997 European Forum, The Royal Aeronautical Society, Wind Tunnels and Wind Tunnel Test Techniques, Cambridge, UK, April 14–16, 1997.
21. W. Sutherland, 'The viscosity of gases and molecular force', *Phil. Mag.*, **5**, 507–531 (1893).
22. B. Mohammadi, 'Fluids Dynamics Computation with NSC2KE A User Guide Release 1.0', RT-0164, INRIA, May 1994.
23. J.O. Hinze, *Turbulence: An Introduction to its Mechanics and Theory*, McGraw Hill, New York, pp. 352, 1959.
24. E.L. Houghton and P.W. Carpenter, *Aerodynamics for Engineering Students*, 4th ed., Edward Arnold, London, 1993.
25. C.A.J. Fletcher, *Computational Techniques for Fluid Dynamics*, Springer, New York, 1990.
26. R.J. Adrian, 'Particle-tracking techniques for experimental fluid mechanics', *Annu. Rev. Fluid Mech.*, **23**, 261–304 (1991).
27. P.J. Bryanston-Cross and J.D. Denton, 'Comparison of interferometric measurements and computed flow around a wedge profile in the transonic region', *ASME*, 1982, 82-GT-258.
28. M. Funes-Gallanzi, D.D. Udrea and P.J. Bryanston-Cross, 'Validation and simulation software for PIV data based on CFD', in preparation.

